Control of ultrafast pulses in a hydrogen-filled hollow-core photonic-crystal fiber by Raman coherence

F. Belli,[1,*] A. Abdolvand,[1,†] J. C. Travers,[1,2] and P. St. J. Russell[1]
[1]*Max Planck Institute for the Science of Light, Staudtstrasse 2, 91058 Erlangen, Germany*
[2]*School of Engineering and Physical Sciences, Heriot-Watt University, Edinburgh EH14 4AS, United Kingdom*

(Received 13 March 2017; published 12 January 2018)

We present the results of an experimental and numerical investigation into temporally nonlocal coherent interactions between ultrashort pulses, mediated by Raman coherence, in a gas-filled kagome-style hollow-core photonic-crystal fiber. A pump pulse first sets up the Raman coherence, creating a refractive index spatiotemporal grating in the gas that travels at the group velocity of the pump pulse. Varying the arrival time of a second, probe, pulse allows a high degree of control over its evolution as it propagates along the fiber through the grating. Of particular interest are soliton-driven effects such as self-compression and dispersive wave (DW) emission. In the experiments reported, a DW is emitted at ∼300 nm and exhibits a wiggling effect, with its central frequency oscillating periodically with pump-probe delay. The results demonstrate that a strong Raman coherence, created in a broadband guiding gas-filled kagome photonic-crystal fiber, can be used to control the nonlinear dynamics of ultrashort probe pulses, even in difficult-to-access spectral regions such as the deep and vacuum ultraviolet.

DOI: 10.1103/PhysRevA.97.013814

Introduction. Optical nonlinear effects are typically local whereby nonlinear response of media to optical excitations are described by the instantaneous nonlinear polarization created by the optical excitation itself. However, systems with "memory" where the response to an optical excitation, e.g., refractive index, depends on the prehistory of the excitation in the medium offer a much richer dynamical behavior and open the possibility of all-optical control of ultrashort laser pulses. The temporal duration, central frequency, and timing of ultrafast light fields are crucial parameters in several research areas, such as strong-field physics [1], time-resolved spectroscopy [2], and femtochemistry [3]. Several schemes have recently been used to *control locally* in space or time a given process such as a chemical reaction [4], free-induction decays [5], or even the emission of light pulses via high-harmonic generation [6] or in free electron lasers [7]. Many biological samples and photochemical processes require ultrashort pulses in the deep ultraviolet (DUV; <300 nm) [8], where control techniques as well as high repetition rate sources have proved challenging. Here we report a pump-probe technique that makes use of the long-lived Raman coherence [9–11] ("memory" [12,14]) in hydrogen to provide precise *nonlocal control* of light fields, including the DUV, although the technique is directly transferable to the vacuum ultraviolet (VUV) as well.

The system we use is a gas-filled hollow-core photonic-crystal fiber (HC-PCF), which has proven to be an ideal vessel for enhancing all kinds of gas-laser interactions [13,14]. Kagome-style HC-PCF ("kagome-PCF") in particular has been used to generate bright DUV and VUV dispersive waves from few-μJ ∼50 fs pump pulses in the near infrared [15–17]. Such sources are readily scalable to high average powers using compact high repetition rate fiber lasers [18], providing similar photon fluxes to sources based on high-harmonic generation, and are finding applications in different spectroscopy methods, such as angle-resolved photoemission spectroscopy of topological insulators [19]. Controlling the characteristics of these ultrashort UV-VUV pulses [16,20] is extremely challenging, often requiring the development of new techniques.

At gas pressures of a few atmospheres in a hydrogen-filled kagome-PCF, the coherence time T_2 of the molecular oscillations is on the order of several 100 ps, representing the lifetime of the driven refractive index temporal grating, which is more than 1000 times longer than our pump and probe pulses. In our experiments, a pump pulse first creates a Raman coherence wave—the periodic refractive index temporal grating—and then a probe pulse, arriving within time T_2, is modulated by the fast oscillations with THz modulation frequency. The technique has similarities with the coherent control [21] of plasma dynamics [22] and multiphoton transitions [23]. However, in our work the control technique is highly nonlocal in time and allows us to control ultrashort probe pulses with the same or even greater energy with respect to the driving pump pulse, leading to richer nonlinear dynamics such as pulse compression and broadening, along with the generation of supercontinua and dispersive wave emission and control in the DUV.

Physical model. The propagation of ultrashort pulses is accurately described by the unidirectional pulse propagation equation (UPPE) [24,25], as confirmed both in free-space configurations [24,26] and in waveguide geometries such as hollow dielectric capillaries and PCFs [15–17,25]. The UPPE

*Present address: School of Engineering and Physical Sciences, Heriot-Watt University, Edinburgh EH14 4AS, UK; f.belli@hw.ac.uk
†Present address: School of Electrical and Electronic Engineering, Nanyang Technological University, 50 Nanyang Avenue, 639798 Singapore.

can be written, for the LP_{01}-like core mode, in the form

$$\partial_z \tilde{E}_1(z,\omega) = i\left[\beta(\omega) - \frac{\omega}{v_1}\right]\tilde{E}_1(z,\omega) + \frac{i\omega^2}{2c^2\varepsilon_0\beta(\omega)}\tilde{p}_{11}(z,\omega), \tag{1}$$

where z is the position along the fiber, ω the angular frequency, a tilde above a quantity denotes the temporal Fourier transform, and $E(z,t)$ is the electric field, defined over an effective mode area A_{eff}. The modal longitudinal wave vector component is $\beta(\omega)$, c is the speed of light in vacuum, ε_0 the permittivity of free space, $p_{11}(z,\omega)$ the nonlinear polarization, v_1 the group velocity of a pulse with central frequency at ω_0, and $\tau = t - z/v_1$ is the reduced time in a reference frame moving at velocity v_1.

In order to isolate interpulse effects, we derive a propagation model for the probe pulse by considering two highly delayed pulses:

$$\begin{aligned} E_1(0,t) &= \sqrt{2P_1/(n_{\text{eff}}\varepsilon_0 c A_{\text{eff}})}e^{-t^2/2\tau_p^2}\cos(\omega_0 t), \\ E_2(0,t) &= \sqrt{2P_2/(n_{\text{eff}}\varepsilon_0 c A_{\text{eff}})}e^{-(t-\tau_{\text{in}})^2/2\tau_p^2}\cos(\omega_0 t), \end{aligned} \tag{2}$$

where 1 represents the pump pulse and 2 the delayed pulse. P_i is the peak power of the ith pulse, τ_{p} its duration, and n_{eff} is the effective modal index. The delay τ_{in} between pulses is defined so that $E_1(z,t)E_2(z,t)$ is effectively zero, i.e., $\tau_{\text{in}} \gg \tau_p$. In this highly nonoverlapping limit, the first pulse is described by Eq. (1), but the second pulse obeys the equation

$$\partial_z \tilde{E}_2 = i\left[\beta(\omega) - \frac{\omega}{v_1}\right]\tilde{E}_2 + \frac{i\omega^2}{2c^2\varepsilon_0\beta(\omega)}[\tilde{p}_{12} + \tilde{p}_{22}]. \tag{3}$$

In Eqs. (1) and (3), p_{11} and p_{22} account for any *self-induced* nonlinear polarization waves created by the first and second pulses. This may include any instantaneous and noninstantaneous nonlinear responses such as Kerr-induced self-phase modulation and Raman- and ionization-induced nonlinear polarization, and it can be straightforwardly extended to any sequence of nonoverlapping pulse. Here, p_{12} accounts only for any causal and long-lived (compared to the pump pulse duration) nonlinear polarization acting on the probe pulse. For example, the long-lived Raman coherence or the free-electron density produced by the first pulse may survive to influence the second pulse via the term p_{12}. Note that the Kerr-induced cross-phase modulation ($\propto E_1^2 E_2$ [27]) of the probe pulse does not play any role in p_{12} in Eq. (2), since the two pulses do not overlap in time.

Here we focus our attention on the effect of the long-lived Raman coherence wave, excited impulsively [9–11,15,28] by the pump pulse, on the probe pulse for delays $\tau \gg \tau_{\text{p}}$ but within the lifetime of the Raman coherence wave T_2, i.e., $\tau \ll T_2$. Under these circumstances $p_{12}(z,\tau)$ can be written

$$\begin{aligned} p_{12}(z,\tau) &= 2n_0\varepsilon_0\Delta n_{12}(z,\tau)E_2(z,\tau), \\ \Delta n_{12}(z,\tau) &= \frac{N_{\text{t}}\alpha_{\text{R}}^2}{2n_0\varepsilon_0\hbar}|\tilde{I}(\Omega_{\text{R}},z)|\ \sin(\Omega_{\text{R}}\tau), \end{aligned} \tag{4}$$

where N_{t} is the total molecular density and $\Delta n_{12}(z,\tau)$ is the resulting nonlinear refractive index modulation, which is proportional to the z-dependent intensity spectrum of the pump pulse at the Raman frequency $\Omega_{\text{R}}/2\pi$:

$$\begin{aligned} \tilde{I}(\Omega_{\text{R}},z) &= \int_{-\infty}^{+\infty} dt\, E^2(z,t)e^{i\Omega_R t} \\ &= \frac{1}{2\pi}\int_{-\infty}^{+\infty} d\omega'\,\tilde{E}(\omega',z)\tilde{E}^*(\omega'-\Omega_{\text{R}},z). \end{aligned} \tag{5}$$

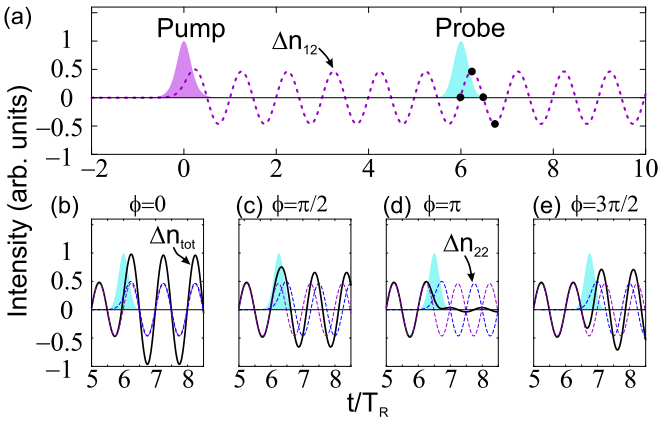

FIG. 1. (a) Pump (purple) and probe (cyan) intensities together with nonlinear modulation of the refractive index induced by the pump Δn_{12} (dashed purple) as a function of the normalized temporal delay τ/T_{R}. (b)–(e) Probe intensity and self-induced Raman nonlinear index induced by the probe (dashed blue, Δn_{22}) and by the pump (dashed purple, Δn_{12}), together with overall Raman nonlinear index $\Delta n_{\text{tot}} = \Delta n_{22} + \Delta n_{12}$.

Figure 1(a) shows the resulting nonlinear refractive index modulation $\Delta n_{12}(0,\tau)$ when the system is driven in the impulsive regime, i.e., $\tau_{\text{p}} \ll T_{\text{R}} = 2\pi/\Omega_{\text{R}}$ [28]. In contrast to glass, where the Raman coherence time T_2 ranges from a few fs in fused silica to ~250 fs in As_2S_3, T_2 in molecular gases ranges from hundreds of ps to a few ns, depending on the gas pressure, making pump-probe measurements with fs-pulses rather straightforward to carry out. Figure 1 illustrates such a pump-probe experiment (numerically modeled), with identical pump and probe pulses, as the delay of the probe is scanned over T_{R}. Figures 1(b)–1(e) show the total nonlinear refractive index modulation $\Delta n_{\text{tot}} = \Delta n_{22} + \Delta n_{12}$ (black curves) for the four different values of τ_{in} marked by black dots in Fig. 1(a). Δn_{tot} carries information on the Raman-induced refractive index change induced both by the first (Δn_{12}) and the second pulses (Δn_{22}). When $\tau_{\text{in}} = mT_{\text{R}}$, where m is an integer, the two Raman responses add (with relative phase $\phi = 0$), so that the probe pulse sees an increasing refractive index in the vicinity of $\tau = \tau_{\text{in}}$. When $\tau_{\text{in}} = (m + \frac{1}{2})T_{\text{R}}$, however, the Raman responses are π out-of-phase [Fig. 1(d)] and the probe pulse sees a decreasing refractive index under its envelope. When $\tau_{\text{in}} = (m + \frac{1}{4})T_{\text{R}}$ the overall Raman response is bell-shaped [Fig. 1(c)], with regions of increasing and decreasing index under the probe pulse envelope.

These refractive index variations strongly affect the dynamics of the probe pulse as it propagates along the fiber [Figs. 2(a)–2(d)]. For $\phi = 0$ it is redshifted, with a steepened trailing edge [Fig. 2(a)]. For $\phi = \pi$ there is an overall blueshift, with a steepened leading edge [Fig. 2(c)], and for $\phi = \pi/2$ there is either pulse compression [Fig. 2(b)] or for $\phi = 3\pi/2$ decompression [Fig. 2(d)].

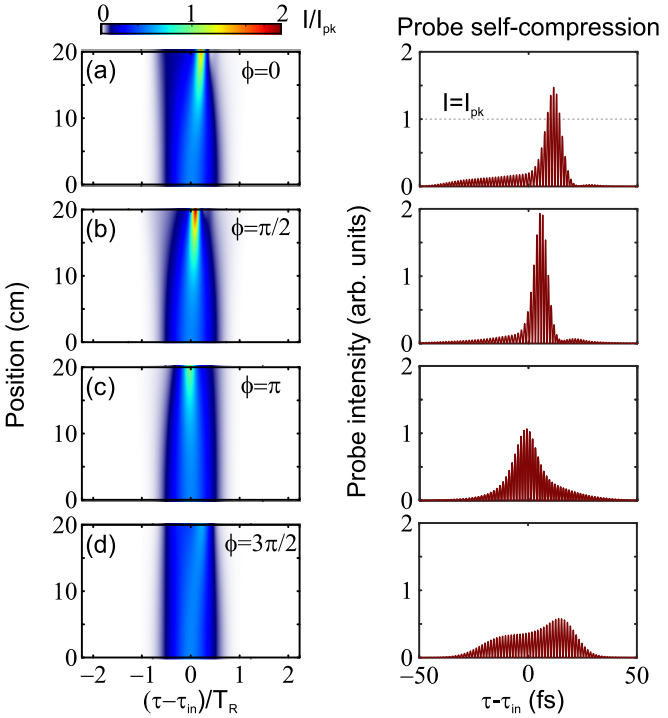

FIG. 2. Left: Numerically simulated probe intensity as a function of time τ/T_R and fiber position for $\tau_{in}/T_R = 6.5$, 7, 7.5, and 8. Right: Snapshots of the probe intensity profile at the fiber output (red lines). All the probe intensities are normalized to the peak pump intensity I_{pk}.

Controlling self-compression of the probe pulse. In the experiment, a pulse shaper (Dazzler) at the fiber input was used to create, and control the delay between, two identical, transform-limited (35 fs) pulses, each with 0.2 μJ energy. These were delivered from a 1 kHz Ti:sapphire laser system with central wavelength at 805 nm. The interpulse delay τ_{in} and pulse shapes at the fiber input were estimated from measured FROG traces. A kagome-PCF, with a flat-to-flat core diameter of 25.3 μm and length of 20 cm, was filled with 7 bars of hydrogen. For these parameters the zero dispersion wavelength is 498 nm, the second-order dispersion is $-3.2\,\mathrm{fs}^2/\mathrm{cm}$, and the pulses undergo moderate soliton self-compression [13,14] with soliton order ~2.

Figure 3(a) shows the experimental spectra collected at the fiber output as a function of the input delay τ_{in}. The spectral fringes observed at each value of τ_{in} arise from the interference of the two pulses in the spectrometer [29,30]. Periodic breathing of the spectral bandwidth, which occurs every $T_R = 57$ fs (the period of the S(1) transition in ortho-hydrogen [31] and marked by vertical lines) is evident as well (note that the duration of the pump and probe pulses is not short enough to excite vibrational transitions in H_2 ($T_R = 8$ fs) as in [15]). The spectral bandwidth reaches its maximum extent for $\tau_{in} = (m + \frac{1}{4})T_R$, as expected from the numerical simulations in Fig. 2(b). There is excellent agreement, without any free parameters, between experiment and numerical modeling, as seen in Fig. 3(b).

The spectral modulation at fixed τ_{in} is caused by spectral interference of the pump and probe fields in the spectrometer,

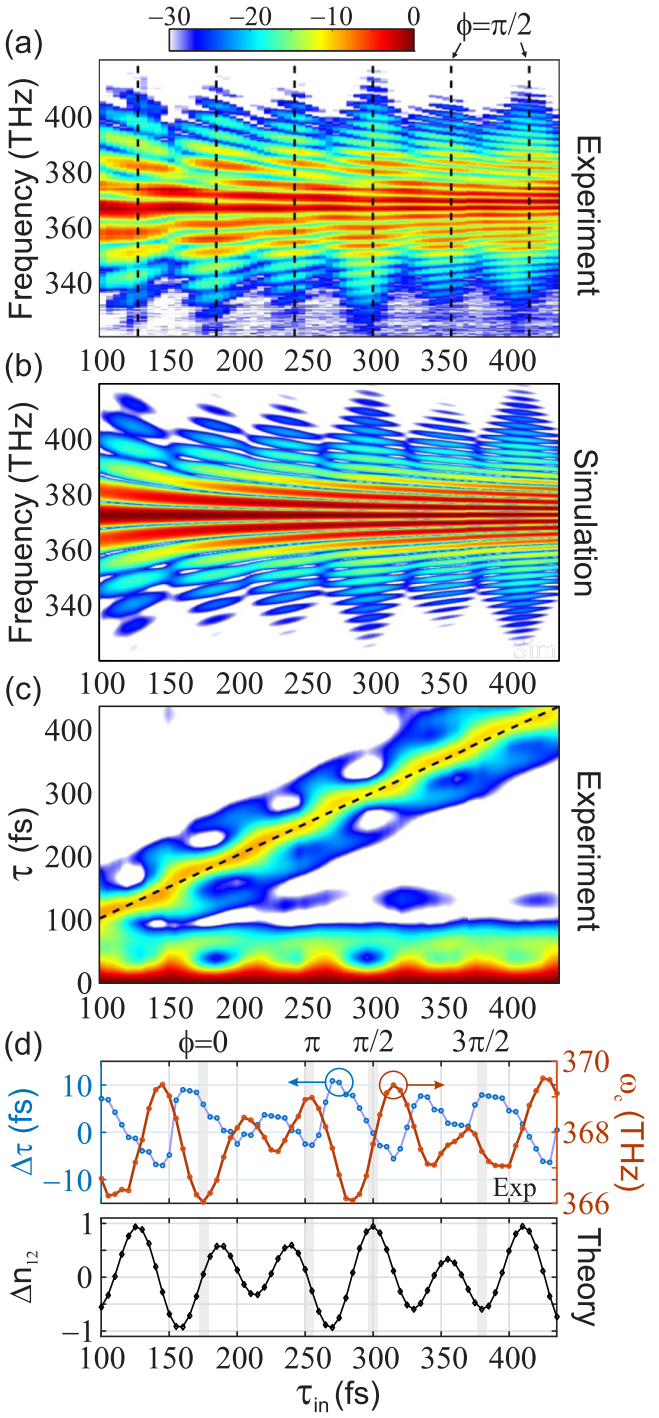

FIG. 3. (a) Experimental spectra at the fiber output as function of τ_{in}. (b) Corresponding numerical simulations. (c) Cross-correlation function $S(\tau;\tau_{in})$ as a function of time and τ_{in}, obtained from the experimental spectra in (a). (d) Lower: Theoretically calculated Raman-related refractive index modulation (black, arb. units). Upper: Calculated central frequency ω_c (red curve, right-hand axis) and temporal delay $\Delta\tau = \tau_{out} - \tau_{in}$ (left-hand axis).

and takes the form [29]

$$\tilde{S}(\omega;\tau_{in}) = |\tilde{E}_1(\omega)|^2 + |\tilde{E}_2(\omega)|^2 + 2|\tilde{E}_1(\omega)||\tilde{E}_2(\omega)|\cos[\varphi_1(\omega) - \varphi_2(\omega)], \quad (6)$$

where $\varphi_1(\omega)$ and $\varphi_2(\omega)$ are the spectral phases of the pump and probe pulses at the fiber output. Equation (6) encodes information on the phase difference between the two pulses. The spectral fringe spacing in Fig. 3(a) is determined by their separation τ_{out} at fiber output. As result of the Raman-related change in the refractive index [Eq. (4)], τ_{out} "wiggles" around τ_{in} with a period that equals T_R, as we will now discuss.

In order to extract information on the relative phase from the observed spectral fringes, and thus the temporal separation between the pulses at the fiber output, we take the inverse Fourier transform of $\tilde{S}(\omega;\tau_{in})$. The resulting function includes the sum of the autocorrelation functions of the pump and the probe pulses, $I_{ac}(\tau;\tau_{in}) = E_1 * E_1 + E_2 * E_2$, and twice their cross-correlation $I_{xc}(\tau;\tau_{in}) = E_1 * E_2$, where $*$ represents the convolution and τ is the pulse separation at the fiber output, estimated from the fringe spacing in Fig. 3(a). Figure 3(c) plots $S(\tau;\tau_{in}) = I_{ac}(\tau;\tau_{in}) + 2I_{xc}(\tau;\tau_{in})$, calculated from the experimental data in Fig. 3(a). Since the cross- and auto-correlations are even functions of τ, we plot only the $\tau > 0$ part. It consists of a contribution at $\leqslant \tau_p/2$ and two contributions centered at $|\tau| \sim \tau_{in}$. $I_{ac}(\tau;\tau_{in})$ maps the periodic change in probe pulse duration, which is inversely related to the spectral bandwidth breathing observed in Fig. 3(a). On the other hand, $I_{xc}(\tau;\tau_{in})$ maps the relative phase difference, and thus the temporal spacing, at the fiber output. The black dashed line in Fig. 3(c) is for $\tau = \tau_{in}$. It is evident that I_{xc} has a peak at $|\tau| \sim \tau_{in}$. Defining the position of the peak as the actual temporal separation τ_{out} between the two pulses at the fiber output (i.e., the reciprocal of the spectral fringe spacing), it is clear from Fig. 3(c) that τ_{out} oscillates around τ_{in}. Note that the increase in probe bandwidth is commensurate with its reduced pulse duration.

Figure 3(d) plots $\Delta\tau = \tau_{out} - \tau_{in}$ versus τ_{in}, highlighting the acceleration ($\Delta\tau < 0$) and deceleration ($\Delta\tau > 0$) experienced by the probe pulse during propagation [32] and caused by pump-induced rotational coherence. Since the pump pulse is short enough to excite rotational Raman coherence in both para- and ortho-hydrogen, both contributions must be taken into account for a complete explanation of the observed dynamics. Fourier analysis of $\Delta\tau(\tau_{in})$ reveals two strong sidebands centered at 10 ± 1 THz and 17 ± 1 THz, which match the rotational S(1)-transitions of ortho- and para-hydrogen, centered at 17.6 and 10.8 THz, respectively. Figure 3(d) shows (black line, lower panel) the expected overall modulation of nonlinear refractive index due to the cross-term:

$$\Delta n_{12}(z,\tau) = \frac{N_t \alpha_R^2}{2n_0\varepsilon_0\hbar}[w_{para}\tilde{I}(\Omega_{para},z)\sin(\Omega_{para}\tau) + w_{ortho}\tilde{I}(\Omega_{ortho},z)\sin(\Omega_{ortho}\tau)]. \quad (7)$$

Equation (7) now includes both para- and ortho-hydrogen contributions—as compared to Eq. (4)—where $w_{para} = 0.33$ and $w_{ortho} = 0.67$ are the relative populations of para- and ortho-hydrogen under standard conditions. The oscillation of the mean central frequency $\omega_c(\tau_{in})$, obtained from the spectra in Fig. 3(a) and plotted as the orange curve in Fig. 3(d), fits well to the value estimated from Eq. (6) [Fig. 3(d), black curve].

From the experimental curves we observe an increase in the redshift and probe deceleration for $\phi = 0$, while for $\phi = \pi$ we observe a blueshift and probe acceleration. The maximum

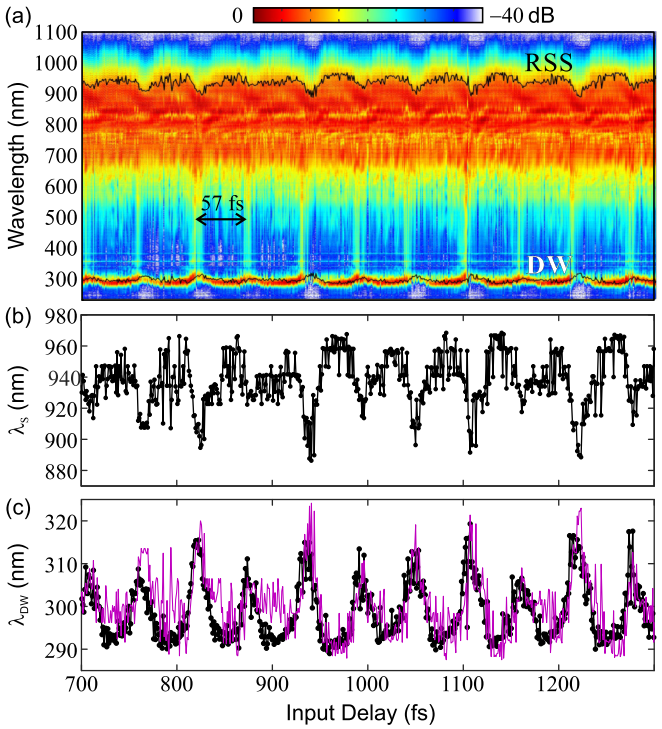

FIG. 4. (a) Experimental spectra collected at the fiber output, plotted against the pump-probe delay τ_{in} at the fiber input. (b) The wavelength λ_s of the strongest redshifted part of the spectrum (RSS). (c) The central wavelength λ_{DW} of the UV dispersive wave (black). The purple line is the DW wavelength, calculated assuming λ_s is the central wavelength of the compressed probe pulse.

spectral bandwidth and minimum temporal duration of the I_{ac} contribution is observed for $\phi = \pi/2$, and the minimum bandwidth and largest duration for $\phi = 3\pi/2$, in complete agreement with the numerical simulations shown in Figs. 2(a)–2(d).

Dispersive wave wiggling. We now discuss interpulse effects that occur when the input pulse undergoes strong soliton self-compression, resulting in the generation of a supercontinuum (SC) and emission of a dispersive wave. The experimental parameters were chosen so that both pulses had soliton order ~5. In contrast to the previous case, however, the pump pulse carried slightly less energy so as to avoid pulse breakup and dispersive wave (DW) emission, with the result that the observed DW dynamics originated entirely from the delayed probe pulse. Using a dispersion-balanced Mach-Zehnder interferometer as pulse shaper, we increased the temporal resolution to 1 fs and widened the range of the interpulse delay to 3 ps. The resulting spectra, obtained in a 20 cm length of kagome-PCF with a 28 μm core diameter and filled with 15 bars of hydrogen, are plotted as a function of input delay in Fig. 4(a). Both pulses are well within the anomalous dispersion regime, and the pump pulse with energy 0.5 μJ, and the probe pulse 0.6 μJ. The pressure was chosen so as to simplify the detection of the emitted DW, which is at ~300 nm, well within the spectral range (200 to 1100 nm) of the CCD-based spectrometer. The fiber length and pulse energies were also optimized experimentally to obtain DW emission at a position as close as possible to the fiber end, so as to avoid any further nonlinear evolution of the DW [15].

A complex periodic modulation of the spectra is observed as a function of interpulse delay, spanning the whole spectrum (300 to 1100 nm). There is a periodic enhancement of the spectral power at longer wavelengths (800 to 1100 nm) and a corresponding oscillation of the central frequency of the ∼300 nm DW band. A SC spectrum, flat to better than 20 dB, is clearly observed every 57 fs (ortho-hydrogen), as shown in Fig. 4.

To understand these dynamics, we plot the delay dependence of the wavelength λ_s of the strongest contribution at wavelengths longer than 800 nm [Fig. 4(a)], and the mean wavelength of the emitted DW [Fig. 4(b)]. Taking λ_s to be the effective central wavelength of the compressed probe pulse, the wavelength of the emitted DW can be estimated from phase matching [purple curve in Fig. 4(b)] [14]. The more the compressed pulse is decelerated (redshifted) the larger is the acceleration (blueshift) of the DW, which empirically explains the anticorrelation observed between λ_s and λ_{DW} in Fig. 4. As τ_{in} is varied, the redshift and blueshift oscillate with a period given by the $2\pi/\Omega_R$. We remark that this wiggling of the DW frequency is a general phenomenon that will occur in many different experiments, including those involving the breakup of a single pulse [15].

Conclusions. The nonlinear dynamics of a probe pulse, including self-compression, supercontinuum generation, and dispersive wave emission, can be simply controlled by varying its time delay relative to a pump pulse that creates coherent Raman oscillations in a hydrogen-filled kagome-PCF. Excellent agreement is obtained between experiment, analytical theory, and numerical simulations. This system offers a versatile highly noninstantaneous means of controlling of the dynamics of ultrashort pulses in a gas-filled PCF—for example, in pulse compression and spectral broadening of DUV light and VUV emission, which are of paramount importance in time-resolved molecular spectroscopy [33] and condensed matter photoemission studies [34]—as well as showing a nonlinear interaction regime among highly nonoverlapping ultrashort pulses mediated by the molecular coherence.

[1] T. Brabec, editor, *Strong Field Laser Physics* (Springer, New York, NY, 2008).
[2] A. M. Weiner, D. E. Leaird, G. P. Wiederrecht, and K. A. Nelson, Science **247**, 1317 (1990).
[3] N. Bloembergen and A. H. Zewail, J. Phys. Chem. **88**, 5459 (1984).
[4] B. J. Sussman, D. Townsend, M. Y. Ivanov, and A. Stolow, Science **314**, 278 (2006).
[5] S. Bengtsson *et al.*, Nat. Photonics **11**, 252 (2017).
[6] T. Pfeifer, R. Kemmer, R. Spitzenpfeil, D. Walter, C. Winterfeldt, G. Gerber, and C. Spielmann, Opt. Lett. **30**, 1497 (2005).
[7] K. C. Prince *et al.*, Nat. Photonics **10**, 176 (2016).
[8] A. Cannizzo, Phys. Chem. Chem. Phys. **14**, 11205 (2012).
[9] S. Baker, I. A. Walmsley, J. W. G. Tisch, and J. P. Marangos, Nat. Photonics **5**, 664 (2011).
[10] N. Zhavoronkov and G. Korn, Phys. Rev. Lett. **88**, 203901 (2002).
[11] V. P. Kalosha and J. Herrmann, Phys. Rev. A **68**, 023812 (2003).
[12] P. J. Bustard, R. Lausten, D. G. England, and B. J. Sussman, Phys. Rev. Lett. **111**, 083901 (2013).
[13] P. St. J. Russell, P. Hölzer, W. Chang, A. Abdolvand, and J. C. Travers, Nat. Photonics **8**, 278 (2014).
[14] J. C. Travers, W. Chang, J. Nold, N. Y. Joly, and P. St. J. Russell, J. Opt. Soc. Am. B **28**, A11 (2011).
[15] F. Belli, A. Abdolvand, W. Chang, J. C. Travers, and P. St. J. Russell, Optica **2**, 292 (2015).
[16] N. Y. Joly, J. Nold, W. Chang, P. Hölzer, A. Nazarkin, G. K. L. Wong, F. Biancalana, and P. St. J. Russell, Phys. Rev. Lett. **106**, 203901 (2011).
[17] A. Ermolov, K. F. Mak, M. H. Frosz, J. C. Travers, and P. St. J. Russell, Phys. Rev. A **92**, 033821 (2015).
[18] C. Jauregui, J. Limpert, and A. Tunnermann, Nat. Photonics **7**, 861 (2013).
[19] H. Bromberger, A. Ermolov, F. Belli, H. Liu, F. Calegari, M. Chávez-Cervantes, M. T. Li, C. T. Lin, A. Abdolvand, P. S. J. Russell, A. Cavalleri, J. C. Travers, and I. Gierz, Appl. Phys. Lett. **107**, 091101 (2015).
[20] I. Cristiani, R. Tediosi, L. Tartara, and V. Degiorgio, Opt. Express **12**, 124 (2004).
[21] W. S. Warren, H. Rabitz, and M. Dahleh, Science **259**, 1581 (1993).
[22] Z.-H. He, B. Hou, V. Lebailly, J. A. Nees, K. Krushelnick, and A. G. R. Thomas, Nat. Commun. **6**, 7156 (2015).
[23] D. Meshulach and Y. Silberberg, Phys. Rev. A **60**, 1287 (1999).
[24] M. Kolesik and J. V. Moloney, Phys. Rev. E **70**, 036604 (2004).
[25] F. Tani, J. C. Travers, and P. St. J. Russell, J. Opt. Soc. Am. B **31**, 311 (2014).
[26] L. Bergé, S. Skupin, R. Nuter, J. Kasparian, and J.-P. Wolf, Rep. Prog. Phys. **70**, 1633 (2007).
[27] R. R. Alfano, *The Supercontinuum Laser Source: The Ultimate White Light*, 3rd ed. (Springer, New York, NY, 2016).
[28] Y.-X. Yan, E. B. Gamble, and K. A. Nelson, J. Chem. Phys. **83**, 5391 (1985).
[29] L. Lepetit, G. Cheriaux, and M. Joffre, J. Opt. Soc. Am. B **12**, 2467 (1995).
[30] M. Takeda, H. Ina, and S. Kobayashi, J. Opt. Soc. Am. **72**, 156 (1982).
[31] M. J. Weber, *CRC Handbook of Laser Science and Technology Supplement 2: Optical Materials*, 1st ed. (CRC Press, Boca Raton, 1994).
[32] M. F. Saleh, A. Armaroli, T. X. Tran, A. Marini, F. Belli, A. Abdolvand, and F. Biancalana, Opt. Express **23**, 11879 (2015).
[33] S. Mukamel, Annu. Rev. Phys. Chem. **41**, 647 (1990).
[34] A. Damascelli, Z. Hussain, and Z.-X. Shen, Rev. Mod. Phys. **75**, 473 (2003).